IL NUOVO CIMENTO Vol. 37 C, N. 6 Novembre-Dicembre 2014
DOI 10.1393/ncc/i2015-11847-0

Colloquia: LaThuile14

Heavy flavor and spectroscopy in CMS

S. Fiorendi on behalf of the CMS Collaboration
Università di Milano - Bicocca and INFN, Sezione di Milano - Bicocca - Milano, Italy

ricevuto il 31 Luglio 2014

Summary. — Selected measurements in the Heavy Flavor sector based on proton proton data collected at $\sqrt{s} = 7$ and 8 TeV by the CMS experiment are reviewed. We report on the measurement of the χ_{b2} over χ_{b1} cross-section ratio and of the relative B_c branching fractions. The observation of peaking structures in the $J\psi\phi$ mass spectrum is also presented. Finally, we report on the search for a new bottomonium state decaying to $\Upsilon(1S)\pi^+\pi^-$.

PACS 13.25.-k – Hadronic decays of mesons.
PACS 14.40.Nd – Bottom mesons ($|B| > 0$).
PACS 14.40.Nd – Heavy quarkonia.

1. – Introduction

In this report we summarize some recent measurements from the CMS experiment [1] at the Large Hadron Collider concerning the production of Heavy Flavors and the search for new exotic states.

2. – Measurement of the χ_{b2} over χ_{b1} cross-section ratio

The χ_{b2} over χ_{b1} cross-section ratio is measured using 20.7 fb^{-1} of data collected at $\sqrt{s} = 8$ TeV [2]. The small difference between the χ_{b1} and χ_{b2} masses (19.4 MeV) and the small χ_b production cross-section constitutes a challenge for the detector performance.

The analysis has been carried out in analogy with the previous CMS measurement in the χ_c sector [3]. The χ_{b2} and χ_{b1} states are reconstructed through their radiative decays $\chi_{b1,2}(1P) \to \Upsilon(1S) + \gamma$, where the $\Upsilon(1S)$ subsequently decays into two muons. The conversion of the low-energy photons produced in the decay results in quite soft and often rather asymmetric electron and positron tracks. The selected $\Upsilon(1S)$ and converted photons are paired to form χ_b candidates. The invariant mass of the χ_b candidate is then calculated through a kinematic fit, which constrains the invariant mass of the dimuon to the $\Upsilon(1S)$ mass and the electron-positron invariant mass to zero. The small mass resolution needed to resolve the two χ_b states is obtained by measuring the photon energy

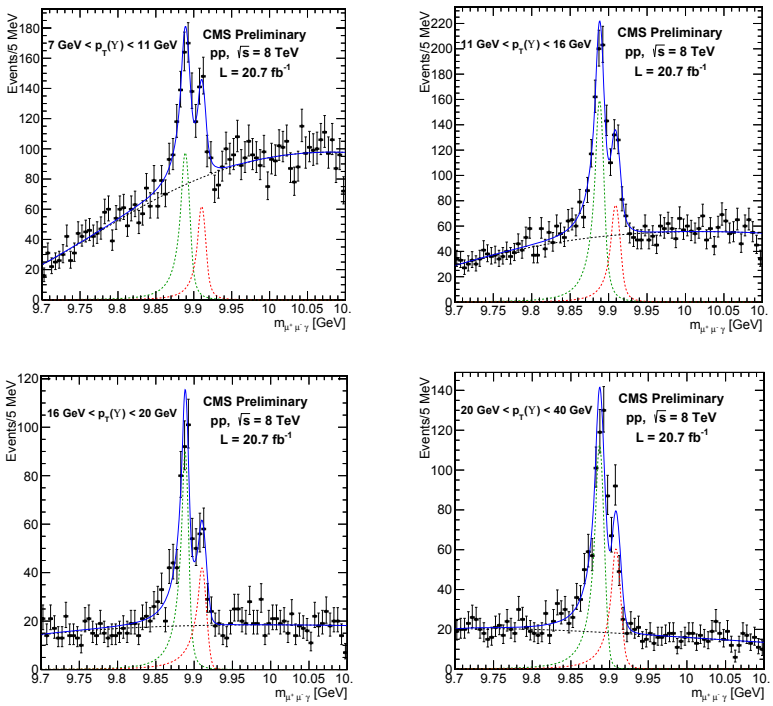

Fig. 1. – Invariant-mass distributions of the χ_b candidates for each of the four $\Upsilon(1S)$ p_T bins considered in the analysis.

from the reconstruction of the momenta of the electron-positron pair originating from its conversion in the beam pipe or in the inner layers of the CMS silicon tracker. However, given the low conversion probability and reconstruction efficiency for low-energy photons, this entails a small yield for the χ_b signals.

The results are presented in four intervals of $\Upsilon(1S)$ transverse momentum in the range 7–40 GeV. The corresponding χ_b signals are shown in fig. 1 for the four bins respectively. A reliable parametrization of the signal shape is inferred from the MC simulation.

For each of the four p_T^Υ bins, the cross-section ratio is calculated as

$$R = \frac{\sigma(pp \to \chi_{b2} + X)}{\sigma(pp \to \chi_{b1} + X)} = \frac{N_{\chi_{b2}}}{N_{\chi_{b1}}} \cdot \frac{\epsilon_1}{\epsilon_2} \cdot \frac{\mathcal{B}(\chi_{b1}(1P) \to \Upsilon(1S) + \gamma)}{\mathcal{B}(\chi_{b2}(1P) \to \Upsilon(1S) + \gamma)}, \tag{1}$$

where $N_{\chi_{b1,2}}$ are the yields of $\chi_{b1,2}$ signal candidates, simultaneously obtained from an unbinned maximum-likelihood (UML) fit to the dimuon-photon invariant-mass spectrum, $\epsilon_{1,2}$ are the acceptance and efficiency corrections obtained from the simulation, and $\mathcal{B}(\chi_{b1,2}(1P) \to \Upsilon(1S) + \gamma)$ are the branching fractions of the corresponding radiative decays [4].

Several sources of systematic uncertainties have been investigated. In particular, effects due to the signal parametrization and to the limited size of the MC samples have been evaluated. Systematic uncertainties arising from generated $\chi_{b1,2}$ p_T spectra have been addressed. An additional relative uncertainty on the ratio of the branching fractions is also considered.

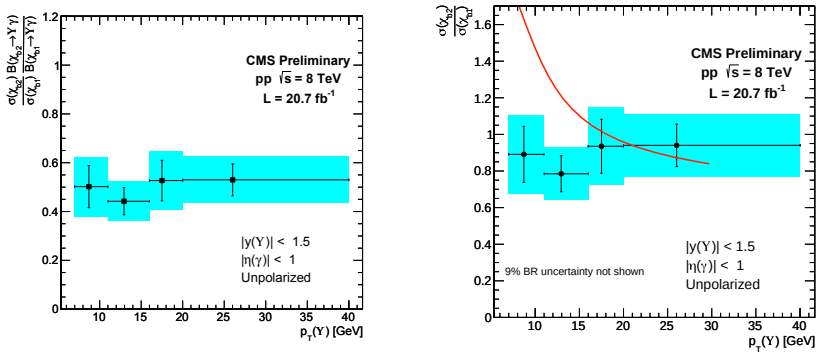

Fig. 2. – Measured χ_{b2} over χ_{b1} cross-section ratio as a function of p_T^{Υ} before (left) and after (right) correcting for the ratio of the branching fractions of the decay channels to $\Upsilon(1S)+\gamma$. The error bars represent statistical uncertainties and the colored bands represent total uncertainties. The uncertainty of the ratio of branching fractions is not explicitly added.

The resulting χ_{b2} over χ_{b1} cross-section ratio is shown in fig. 2 before (left) and after (right) the correction for the ratio of the branching fractions of the decay channels to $\Upsilon(1S)+\gamma$. The solid curve in the right plot shows the theoretical prediction extracted from [5].

3. – Measurement of the B_c branching fractions

The $B_c^{\pm} \to J/\psi\pi^{\pm}$ and $B_c^{\pm} \to J/\psi\pi^{\pm}\pi^{\pm}\pi^{\mp}$ decay modes are studied in the kinematic region where the transverse momentum of the $B_c^{\pm}$ meson is greater than 15 GeV and within the central rapidity region $|y| < 1.6$ [6]. We present the measurement of the ratio of the two hadronic decay branching fractions $\frac{\mathcal{B}(B_c^{\pm}\to J/\psi\pi^{\pm}\pi^{\pm}\pi^{\mp})}{\mathcal{B}(B_c^{\pm}\to J/\psi\pi^{\pm})}$. The $B_c^{\pm} \to J/\psi\pi^{\pm}$ mode is also compared to the topologically similar decay $B^{\pm} \to J/\psi K^{\pm}$, and the ratio of the production cross-section times branching fraction $\frac{\sigma(B_c^{\pm})\times\mathcal{B}(B_c^{\pm}\to J/\psi\pi^{\pm})}{\sigma(B^{\pm})\times\mathcal{B}(B^{\pm}\to J/\psi K^{\pm})}$ is measured.

The analysis is based on the 2011 data sample collected at $\sqrt{s} = 7$ TeV, corresponding to an integrated luminosity of 5.1 fb^{-1}. The B_c candidate reconstruction is driven by the J/ψ meson identification through its decay into a dimuon pair. One or three tracks are then associated to the J/ψ to form a B_c candidate. After the vertex fit, which constrains the dimuon mass to the J/ψ nominal one, additional quality cuts are applied to improve the signal to noise ratio. The resulting signals for the $B_c^{\pm} \to J/\psi\pi^{\pm}\pi^{\pm}\pi^{\mp}$, $B_c^{\pm} \to J/\psi\pi^{\pm}$ and $B^{\pm} \to J/\psi K^{\pm}$ channels are shown in fig. 3.

The two ratios are obtained through the relations

$$\frac{\mathcal{B}(B_c^{\pm} \to J/\psi\pi^{\pm}\pi^{\pm}\pi^{\mp})}{\mathcal{B}(B_c^{\pm} \to J/\psi\pi^{\pm})} = \frac{N_{3\pi}}{N_{\pi}} \cdot \frac{\epsilon_{\pi}}{\epsilon_{3\pi}} \tag{2}$$

and

$$\frac{\sigma(B_c^{\pm}) \cdot \mathcal{B}(B_c^{\pm} \to J/\psi\pi^{\pm})}{\sigma(B^{\pm}) \cdot \mathcal{B}(B^{\pm} \to J/\psi K^{\pm})} = \frac{N_{\pi}}{N_B} \cdot \frac{\epsilon_B}{\epsilon_{\pi}} \tag{3}$$

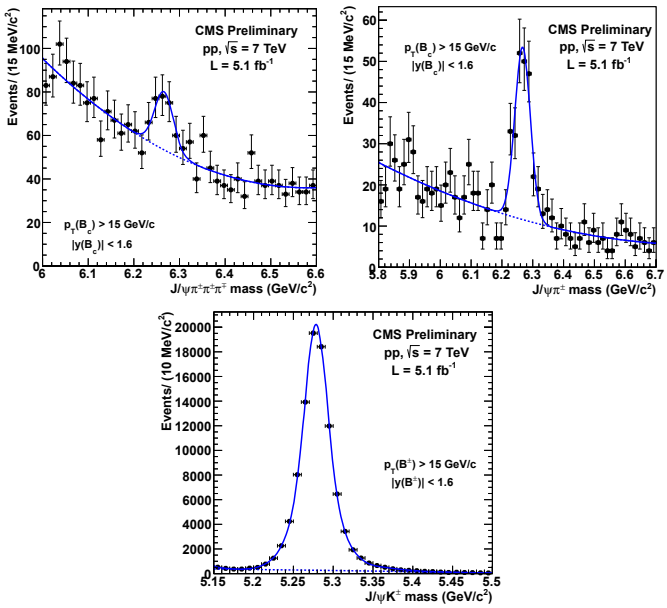

Fig. 3. – Invariant-mass distribution of $B_c^{\pm} \to J/\psi\pi^{\pm}\pi^{\pm}\pi^{\mp}$, $B_c^{\pm} \to J/\psi\pi^{\pm}$ and $B^{\pm} \to J/\psi K^{\pm}$ candidates, respectively.

where $N_{3\pi}$, N_{π} and N_B are the numbers of signal events, $\epsilon_{3\pi}$, ϵ_{π} and ϵ_B are the overall analysis efficiencies (including acceptance, reconstruction, selection and trigger efficiency) evaluated on the MC for the reconstruction of the $B_c^{\pm} \to J/\psi\pi^{\pm}\pi^{\pm}\pi^{\mp}$, $B_c^{\pm} \to J/\psi\pi^{\pm}$ and $B^{\pm} \to J/\psi K^{\pm}$ channels respectively.

The efficiencies for the $B_c^{\pm} \to J/\psi\pi^{\pm}$ and $B^{\pm} \to J/\psi K^{\pm}$ channels are measured as a function of the candidate transverse momentum and computed in transverse-momentum bins, whose size is determined by the available MC statistics.

The efficiency for the $B_c^{\pm} \to J/\psi\pi^{\pm}\pi^{\pm}\pi^{\mp}$ mode has been estimated following a different approach. The five-body decay can involve intermediate resonant states; the quantitative determination of resonant contributions and their interferences would require a sophisticated amplitude analysis which is not feasible with the available statistics. In order to take into account possible effects of the decay dynamics on the reconstruction efficiency, a model-independent efficiency treatment has been developed: the five-body decay of a spinless particle can be fully described in its center of mass by 8 independent mass-combinations of the type m_{ij} $(i \neq j)$, where m_{ij} is the squared invariant mass of the pair of particles i and j in the final state. In the present case, the additional J/ψ mass constraint reduces to 7 the number of independent m_{ij}. The following seven mass-combinations have been chosen: $x = m^2(\mu^+\pi^+)_{low}$, $y = m^2(\pi^+\pi^-)_{high}$, $z = m^2(\mu^+\pi^-)$, $w = m^2(\pi^+\pi^+)$, $r = m^2(\mu^-\pi^+)_{low}$, $t = m^2(\mu^-\pi^+)_{high}$ and $v = m^2(\mu^-\pi^-)$, where the *low* and *high* subscript refers to the lower and higher invariant mass combination where a π^+ is involved. The efficiency is then parametrized as a linear function of the type:

$$\epsilon = \left|p_0 + p_1 \cdot x + p_2 \cdot y + p_3 \cdot z + p_4 \cdot w + p_5 \cdot r + p_6 \cdot t + p_7 \cdot v\right|, \tag{4}$$

where p_i are the free parameters to be determined via an UML fit on the generated events in the 7-dimensional space through a binomial probability.

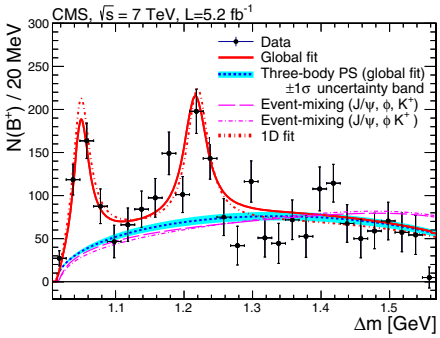

Fig. 4. – Number of $J/\psi\phi K^{\pm}$ candidates as a function of Δm. The solid curve is the global UML fit to data, and the dotted curve is the background contribution assuming three-body PS.

Different sources of systematic uncertainties have been evaluated, namely, contributions due to the fitting technique, uncertainty on the efficiency evaluation due to the MC finite size, possible effects of the efficiency binning and of the efficiency function parametrization, and possible effects coming from the different data-taking conditions. Additional contributions concerning the uncertainty on the tracking efficiency and the experimental uncertainty on the B_c lifetime have been computed.

The resulting values for the ratios are $\frac{\mathcal{B}(B_c^{\pm}\to J/\psi\pi^{\pm}\pi^{\pm}\pi^{\mp})}{\mathcal{B}(B_c^{\pm}\to J/\psi\pi^{\pm})} = 2.43\pm0.76(\text{stat})^{+0.46}_{-0.44}(\text{syst})$ and $\frac{\sigma(B_c^{\pm})\times\mathcal{B}(B_c^{\pm}\to J/\psi\pi^{\pm})}{\sigma(B^{\pm})\times\mathcal{B}(B^{\pm}\to J/\psi K^{\pm})} = [0.48\pm0.05(\text{stat})\pm0.04(\text{syst})^{+0.05}_{-0.03}\ (\tau_{B_c})]\times10^{-2}$.

4. – Observation of peaking structures in the $J/\psi\phi$ mass spectrum in B decays

A study of the $J/\psi\phi$ mass spectrum from $B^{\pm}\to J/\psi\phi K^{\pm}$ decay is reported. The analysis is based on $5.2\pm0.1\,\text{fb}^{-1}$ of data collected in 2011 [7].

Events containing non-prompt J/ψ candidates from B mesons decays are selected and the $B^{\pm}\to J/\psi\phi K^{\pm}$ candidates are formed by combining three additional tracks consistent with the displaced J/ψ vertex and with a total charge of ±1. The vertex fit, constraining the dimuon mass to the J/ψ nominal mass, is performed and quality cuts are applied. The lower invariant mass K^+K^- combination is required to lie within the ϕ mass window. The invariant-mass spectrum of selected $J/\psi\phi K^{\pm}$ candidates is fit with a Gaussian signal function and a second-degree polynomial background function, and returns a B^+ yield of $2480\pm160(\text{stat})$ events.

To investigate the $J/\psi\phi$ invariant-mass spectrum, the $J/\psi\phi K^{\pm}$ candidates are divided into 20 MeV-wide $\Delta m = m(\mu^+\mu^-K^+K^-) - m(\mu^+\mu^-)$ intervals and the corresponding B^+ signal yield is extracted through a fit. The resulting Δm distribution is shown in fig. 4. The mass-difference region $\Delta m > 1.568\,\text{GeV}$ is excluded from the analysis to avoid potential background from $B_s\to\psi(2S)\phi\to J/\psi\pi^+\pi^-\phi$ decays.

Two peaking structures are observed above the simulated phase-space continuum distribution. A full amplitude analysis is not affordable due to the low statistics available.

The Δm distribution is fit with S-wave relativistic Breit-Wigner (BW) functions convolved with a Gaussian mass resolution function. The continuum is parametrized with a three-body phase space shape.

The mass and width of the two structures are extracted by performing a global UML fit to the $J/\psi\phi K^{\pm}$ invariant mass in each Δm interval, in which the B^+ yield is expressed as the product of the relative efficiency times the number of signal events from the two BWs and the nonresonant continuum events.

Systematic uncertainties have been evaluated and concern the choice of the signal and background probability density functions, uncertainties in the shape of the relative efficiency versus Δm and on the Δm background shape, uncertainties caused by the Δm binning and by the Δm mass resolution. Systematic errors arising from selection requirements have also been investigated.

The fit returns a yield of 310 ± 70(stat) and 418 ± 170(stat) events for the lower and higher mass structures, respectively. The corresponding mass and width values are: $m_1 = 4148.0 \pm 2.4(\text{stat}) \pm 6.3(\text{syst})$ MeV, $\Gamma_1 = 28^{+15}_{-11}(\text{stat}) \pm 19(\text{syst})$ MeV; $\Delta m_2 = 4313.8 \pm 5.3(\text{stat}) \pm 7.3(\text{syst})$ MeV, $\Gamma_2 = 38^{+30}_{-15}(\text{stat}) \pm 16(\text{syst})$ MeV. The significance for the lower-mass structure is evaluated to be greater than 5 standard deviations. Because of possible reflections from two-body decays, the statistical significance of the second structure cannot be reliably estimated.

5. – Search for a new bottomonium state decaying to $\Upsilon(1S)\pi^+\pi^-$

A search for the bottomonium counterpart of the $X(3872)$ exotic resonance has been performed using a data sample of $20.7\,\text{fb}^{-1}$ collected at $\sqrt{s} = 8\,\text{TeV}$ in 2012 [8]. Several known properties of the $X(3872)$ state provide clues in the search for the X_b: in particular, the X_b is expected to be a narrow resonance, with a sizable decay rate into $\Upsilon(1S)\pi^+\pi^-$. The strategy of the analysis is therefore to look for a narrow peak, other than the known $\Upsilon(2S)$ and $\Upsilon(3S)$ resonances, in the $\Upsilon(1S)(\to \mu^+\mu^-)\pi^+\pi^-$ invariant-mass spectrum. The analysis probes the kinematic region $p_T(\Upsilon(1S)\pi^+\pi^-) > 13.5\,\text{GeV}$ and $|y(\Upsilon(1S)\pi^+\pi^-)| < 2.0$.

The results are presented in terms of R, the relative inclusive production cross sections of the X_b and $\Upsilon(2S)$ states times their decay branching fractions to $\Upsilon(1S)\pi^+\pi^-$ as a function of the X_b mass between 10 and 11 GeV.

Both the $\Upsilon(2S)$ and the X_b are assumed to be produced unpolarized and with the same production mechanism. Furthermore, the X_b events are assumed to have the same dipion mass distribution as the $\Upsilon(2S)$ events.

The $\Upsilon(1S)$ candidate is reconstructed as a pair of opposite charged muons. The $\Upsilon(1S)\pi^+\pi^-$ candidate is then formed by adding two opposite charged tracks and performing a vertex fit, constraining the dimuon mass to the world-average $\Upsilon(1S)$ mass. The selection criteria have been optimized to maximize the expected signal significance in the mass region near the $\Upsilon(2S)$. The data sample has been divided into a "barrel" and an "endcap" region to exploit the better mass resolution and lower background in the barrel region. The $\Upsilon(1S)\pi^+\pi^-$ invariant mass spectrum is shown in fig. 5. No outstanding structures, apart from the $\Upsilon(2S)$ and the $\Upsilon(3S)$, are observed.

The search for the X_b is performed in the mass regions 10.06–10.31 and 10.40–10.99 GeV, excluding the mass intervals around the $\Upsilon(2S)$ and $\Upsilon(3S)$ resonances. The mass of the hypothetical X_b signal is shifted by 10 MeV intervals, leaving the signal strength floating. The signal shape is modeled with a Gaussian function, whose intrinsic width is assumed to be small compared to the detector mass resolution and is fixed to the values obtained from simulation. For each given X_b mass point, the relationship

$$N^{obs}_{X_b} = R \times N^{obs}_{\Upsilon(2S)} \times \frac{\varepsilon_{X_b}}{\varepsilon_{\Upsilon(2S)}} \tag{5}$$

is evaluated, where $N^{obs}_{X_b}$ and $N^{obs}_{\Upsilon(2S)}$ are the observed X_b and $\Upsilon(2S)$ yields, respectively, and ε_{X_b} and $\varepsilon_{\Upsilon(2S)}$ are the corresponding overall efficiencies, estimated from the simulation.

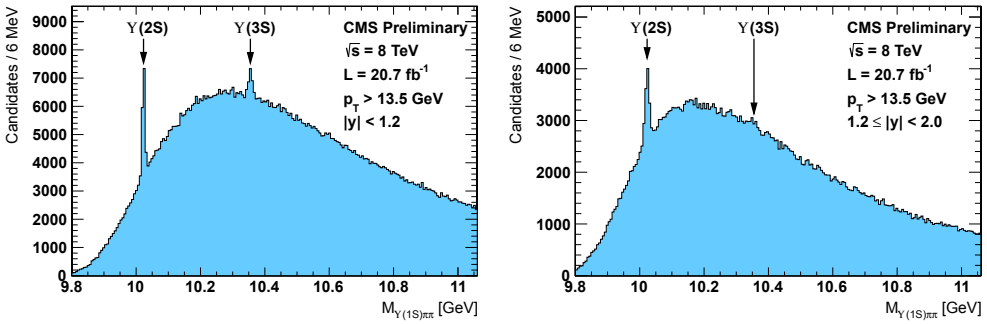

Fig. 5. – Reconstructed invariant mass distributions of the $\Upsilon(1S)\pi^+\pi^-$ candidates in the barrel (left) and endcap (right) regions.

The local p-value is evaluated from simultaneous signal-plus-background fits to the observed invariant-mass distributions in the barrel and endcap regions. Significances of the X_b signal are calculated for each hypothetical X_b mass and an upper limit on R is computed. The expected sensitivity of the analysis is greater than five standard deviations for the explored X_b mass range, if the relative signal strength is comparable to the corresponding value for the $X(3872)$ [9].

Several sources of systematic uncertainties have been considered. The major sources concern the modeling of the signal decay, which includes the dipion invariant mass spectrum and the X_b mass resolution, the signal polarization and the background shape. These systematic uncertainties have been included as nuisance parameters in the p-value calculation, which has been performed using an asymptotic approach. The expected discovery potential is estimated by injecting various amounts of signal events into the fits and evaluating the resulting p-values. The expected and observed p-values are shown in the left plot of fig. 6: no indication of an X_b signal is found. The right plot of fig. 6 shows the observed 95% confidence level upper limits on R, which is the range 0.9–5.4%.

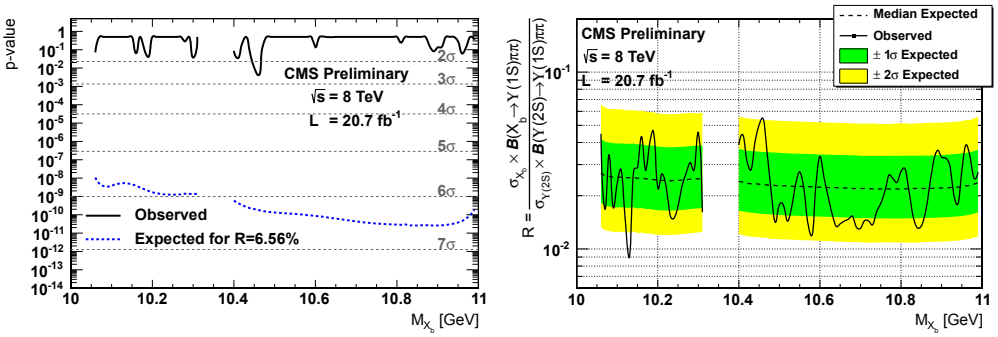

Fig. 6. – Expected and observed local p-values (left) and exclusion limits at 95% confidence level (right) as a function of the injected X_b mass on the ratio R.

6. – Conclusions

A review of some recent results from the CMS experiment has been presented.

The first measurement at a hadron collider of the χ_{b2} and χ_{b1} relative production cross-section has been discussed, and does not show a significant dependence on the $\Upsilon(1S)$ transverse momentum.

The relative branching fraction of the $B_c^{\pm} \to J/\psi\pi^{\pm}\pi^{\pm}\pi^{\mp}$ and $B_c^{\pm} \to J/\psi\pi^{\pm}$ decay modes is measured, in good agreement with the only other available result from the LHCb experiment [10]. Also, we measured the relative production cross-section times the branching ratio for the $B_c^{\pm} \to J/\psi\pi^{\pm}$ and $B^{\pm} \to J/\psi K^{\pm}$ channels in a different kinematical region with respect to the LHCb measurement [11]. This can help in improving theoretical predictions on the B_c production models.

A peaking structure in the $J/\psi\phi$ mass spectrum from $B^{\pm} \to J/\psi\phi K^{\pm}$ decays is observed with a statistical significance greater than 5 standard deviations, and an evidence for a second peaking structure is found in the same mass spectrum. The two structures are above the threshold of open charm decays and have relatively narrow widths, while conventional charmonium mesons with these masses would be expected to have larger widths and to decay mainly into open charm pairs. An angular analysis would help elucidate the nature of these structures but is not affordable with the current statistics.

Finally, we presented the search for an exotic bottomonium state in the decay channel $X_b \to \Upsilon(1S)\pi^+\pi^-$. No significant excess above the background is observed for X_b masses between 10 and 11 GeV and the first upper limits at a hadron collider on the ratio of the inclusive production cross sections times the branching fractions to $\Upsilon(1S)\pi^+\pi^-$ of the X_b and the $\Upsilon(2S)$ are set.

REFERENCES

[1] Chatrchyan S. *et al.* (CMS Collaboration), *JINST*, **3** (2008) S08004.
[2] Chatrchyan S. *et al.* (CMS Collaboration), CMS-PAS-BPH-13-005.
[3] Chatrchyan S. *et al.* (CMS Collaboration), *Eur. Phys. J. C*, **72** (2012) 12.
[4] Particle Data Group Collaboration, *Phys. Rev. D*, **86** (2012) .
[5] Likhoded A. K., Luchinsky A. V. and Poslavsky S. V., *Phys. Rev. D*, **86** (2012) 074027.
[6] Chatrchyan S. *et al.* (CMS Collaboration), CMS-PAS-BPH-12-011.
[7] Chatrchyan S. *et al.* (CMS Collaboration), arXiv:1309.6920, CMS-BPH-11-026, CERN-PH-EP-2013-167, submitted to *Phys. Lett. B*.
[8] Chatrchyan S. *et al.* (CMS Collaboration), *Phys. Lett. B*, **727** (2013) 57.
[9] Chatrchyan S. *et al.* (CMS Collaboration), *JHEP*, **04** (2013) 154.
[10] Aaij R. *et al.* (LHCb Collaboration), *Phys. Rev. Lett.*, **108** (2012) 251802.
[11] Aaij R. *et al.* (LHCb Collaboration), *Phys. Rev. Lett.*, **109** (2012) 232001.